

ENSO response to high-latitude volcanic eruptions in the Northern Hemisphere: the role of the initial conditions

Francesco S.R. Pausata^{1*}, Christina Karamperidou², Rodrigo Caballero¹ and David S. Battisti^{3,4}

Affiliations

¹*Department of Meteorology, Stockholm University and Bolin Centre for Climate Research, Stockholm, Sweden*

²*Department of Atmospheric Sciences, University of Hawaii at Mānoa, Honolulu, HI, USA*

³*Department of Atmospheric Sciences, University of Washington, Seattle, WA, USA*

⁴*UNI Research, Bergen, Norway.*

**Corresponding author: francesco.pausata@misu.su.se*

This article has been accepted for publication and undergone full peer review but has not been through the copyediting, typesetting, pagination and proofreading process which may lead to differences between this version and the Version of Record. Please cite this article as doi: 10.1002/2016GL069575

Abstract:

A large ensemble of Earth System Model simulations is analyzed to show that high-latitude Northern Hemisphere eruptions give rise to El Niño-like anomalies in the winter following the eruption, the amplitude of which depends on the state of the tropical Pacific at the time of the eruption. The El Niño-like anomalies are almost three times larger when the eruption occurs during an incipient La Niña or during a neutral state compared to an incipient El Niño. The differential response results from stronger atmosphere-ocean coupling and extra-tropical feedbacks during an incipient La Niña compared to El Niño. Differences in the response continue through the second and third years following the eruption. When the eruption happens in a year of an incipient El Niño, a large cold (La Niña-like) anomaly develops in year two; if the eruption occurs in a year of an incipient La Niña, no anomalies are simulated in year two and a La Niña-like response appear in year three. After the El Niño-like anomaly in the first winter, the overall tendency of ENSO in the following two years is toward a La Niña state. Our results highlight the high sensitivity of tropical Pacific dynamics under volcanic forcing to the ENSO initial state, and lay the groundwork for improved predictions of the global climatic response to high-latitude volcanic eruptions.

Keywords: *extra-tropical volcanic eruptions / ENSO predictability / initial conditions / tropical Pacific*

Index term: 8408 | 4522 | 1704 | 1724

Key points:

- HL eruptions alter the mean state of ENSO and detectable anomalies are seen up to 3 years after the eruption
- Stronger El Niño-like anomalies on year 1 when eruptions occurs under developing La Niñas
- La Niña-like anomalies on year 2 and year 3 when eruptions occurs under developing El Niños and La Niñas, respectively

1. Introduction

The impacts of high-latitude eruptions on climate are thought to be restricted to the hemisphere of the eruption rather than to be global, because such eruptions generate an aerosol plume that is limited to the hemisphere in which they occur [e.g., *Kravitz and Robock, 2011; Pausata et al., 2015a*]. However, to date only a handful of modeling studies have investigated the climate effects of high-latitude eruptions in detail [*Highwood and Stevenson, 2003; Oman et al., 2005, 2006a; Kravitz and Robock, 2011; Schmidt et al., 2012; Pausata et al., 2015a, 2015b*]. An example of a well-documented destructive high-latitude volcanic eruption in the Northern Hemisphere (NH) is that of Laki (Iceland) in the summer of 1783. The very cold winter of 1783-1784 may have been caused by the Laki eruption, but the mechanisms are not yet well understood [*Schmidt et al., 2012*]. The Laki eruption may also have led to a weakening of the African, Indian and East Asian monsoon circulations (e.g., *Oman et al. [2006]*), causing widespread famine [*Finnsson, 1796; Wood, 1992*]. The two winters following the eruption were extremely cold and snowy across the circum-North Atlantic. A recent study [*D'Arrigo et al., 2011*] questions the relative impact of the 1783 Laki eruption on weather and climate, arguing that natural variability was responsible for the cold 1783-1784 winter. On the other hand, *Pausata et al. [2015b]* used a coupled climate model to demonstrate the potential for large high-latitude eruptions to affect global climate by altering the spatio-temporal characteristics of the El Niño-Southern Oscillation (ENSO) on both short (few years) and long (decades) timescales. The authors showed that large summer high-latitude eruptions in the NH cause an El Niño-like anomaly during the first 8-9 months after the beginning of the eruption. The El Niño-like anomaly is due to the large NH cooling that shifts the Inter-Tropical Convergence Zone (ITCZ) southwards. Such a shift slackens the trade winds along the equator in the western and central Pacific, leading to an El Niño-like

anomaly via the Bjerknes feedback [Bjerknes, 1969]. Hence, the processes leading to El Niño-like anomalies in response to high-latitude NH eruptions were found in Pausata *et al.* [2015b] to be different from those hypothesized to govern the response to tropical eruptions, based on the “dynamical thermostat” mechanism [Hirono, 1988; Clement *et al.*, 1996]. However, there is currently no consensus on the ENSO response to tropical eruptions either from the modeling or the proxy point of view: some studies show El Niño-like anomalies [Adams *et al.*, 2003; Mann *et al.*, 2005; Emile-Geay *et al.*, 2008; Ohba *et al.*, 2013; Maher *et al.*, 2015], while others show La Niña-like anomalies [D’Arrigo *et al.*, 2008; McGregor and Timmermann, 2011] in the winter following the eruption. Still others find no relation between ENSO and volcanic eruptions [Robock, 2000; Ding *et al.*, 2014].

The strength of the ENSO response to volcanic eruptions may depend on the initial state of the ocean [Pausata *et al.*, 2015a, 2015b]; however, no studies have hitherto investigated this hypothesis in the context of high-latitude eruptions. It is well established that knowledge of the atmospheric and ocean state during the preceding seasons can improve ENSO prediction through the causal linkage between summertime sea surface temperature (SST) anomalies in the subtropical North Pacific and ENSO [Vimont *et al.*, 2001; Caballero and Anderson, 2009]. Therefore, improving our knowledge of how the ENSO mode might respond to high-latitude eruptions given its initial state is of considerable importance in understanding and forecasting ENSO evolution in the years following such eruptions.

Here we perform two ensemble simulations of 60 members each (volcano and no-volcano) using a coupled atmosphere-ocean-aerosol model to examine the sensitivity of the ENSO response to high-latitude volcanic eruptions depending on its initial state. This is the first study to investigate this issue using two ensembles with members that start from identical initial conditions and differ only in the volcanic forcing. Previous studies (e.g. [Landrum *et al.*, 2013; Ding *et al.*, 2014; Maher *et al.*, 2015]) used historical simulations or

last millennium simulations with and without volcanic forcing [*Stevenson et al.*, 2016]. However, the experimental designs used in these studies do not include an equivalent run without the volcanic forcing and take as reference period a very short climatology before the eruption (in general 5-6 years), or the volcanic eruptions are imposed without reference to the initial conditions at the same time in the reference simulation. These experimental designs make it more difficult to detect the climatic response (e.g., ENSO or ocean circulation changes) to the volcanic forcing [*Gregory*, 2010; *Pausata et al.*, 2015a] and preclude the possibility of illuminating the sensitivity of the ENSO response to volcanic eruptions vis-à-vis the ENSO phase.

In the present study, we focus our analysis on the short-term (one to three years) ENSO response to a summer NH high-latitude volcanic eruption and the impacts of the initial ENSO state on such a response. The results of this work allow for a better understanding of the sensitivity of tropical Pacific dynamics under volcanic forcing to the ENSO initial state, as well as advance the predictions of the climatic response to such volcanic eruptions.

2. Model Description and Experimental Set-up

We employ the Norwegian Earth System Model (NorESM1-M [*Bentsen et al.*, 2013; *Iversen et al.*, 2013]) to simulate an extreme NH high-latitude multistage eruption using the same experimental design as in *Pausata et al.* [2015a, 2015b]. NorESM1-M has a horizontal resolution of 1.9° (latitude) x 2.5° (longitude) and 26 vertical levels. NorESM1-M uses a modified version of Community Atmospheric Model version 4 (CAM4 [*Neale et al.*, 2013]), CAM4–Oslo to simulate the atmospheric circulation with the updated module that simulates the life cycle of aerosol particles, primary and secondary organics. NorESM1-M includes treatment of the direct effect of aerosols, and the first and second indirect effects of aerosols on warm clouds. The atmospheric model is coupled to the Miami Isopycnic Coordinate Ocean Model – MICOM. A detailed description of the model used in this study can be found

in *Bentsen et al.* [2013], *Iversen et al.* [2013]. With regard to the validation of the simulated sulfate distribution and properties associated to the Laki eruption, the results are presented in detail in Pausata et al. [2015a]. The model is able to reproduce the sulfate concentrations in accordance with a previous modeling study [Oman et al., 2006b], and the climate anomalies simulated after the Laki eruption are in overall agreement with available climate reconstructions (see Pausata et al. [2015a] and references therein).

We simulate the high-latitude eruption by injecting 100 Tg of SO₂ and dust (as an analog for ash) primarily into the upper-troposphere/lower stratosphere over a four-month period. The eruption is comprised of eight injections (sub-eruptions), each lasting for four days and separated by 15 days (see Table 1 in *Pausata et al.* [2015a]). We generate an ensemble of 60 simulations (hereafter referred to as the “volcano ensemble”); each member is initiated with a different year selected from a transient historical simulation (1901-1960), with volcanic eruptions all beginning on June 1st of the first year (YEAR01) and integrated for four years. The no-volcano ensemble is generated simply considering each of the four unperturbed years taken from the historical simulation corresponding to the same years of the perturbed case (e.g., for the volcano experiment starting in 1901 and ending in 1904 the no-volcano member will be composed of the years 1901-1904 from the historical simulation). In our model, we set the start of the eruption in June to mimic the original Laki eruption, which occurred on June 8th 1783 and was one of the strongest high-latitude eruptions in recorded history. In addition, ENSO dynamics have been shown to be especially sensitive to perturbations during the boreal summer [*Thompson and Battisti*, 2000], making the Laki eruption a perfect experimental platform for evaluating impacts on the evolution of ENSO.

To characterize ENSO in the model, we use monthly SST anomalies averaged over the Niño3.4 region (5°N to 5°S, 170°W to 120°W). We apply a 5-month running mean to remove uncoupled intraseasonal variations in SST. We then divide the volcano and no-

volcano ensemble members into three groups according to the incipient ENSO state, where the ENSO state is defined by the terciles of the September through February average Niño3.4 index in the no-volcano control simulation: El Niño (Niño3.4 index $> 0.4^{\circ}\text{C}$), La Niña (Niño3.4 index $< -0.4^{\circ}\text{C}$), and Neutral ($-0.4^{\circ}\text{C} < \text{Niño3.4 index} < 0.4^{\circ}\text{C}$) case. The Niño3.4 index standard deviation is equal to $\sim 0.8^{\circ}\text{C}$. In the remainder of the paper we will use the terms “initial conditions” and “incipient ENSO state” interchangeably in reference to the above-described cases.

Unless otherwise noted, all differences discussed in this study are significant at the 95% confidence level using the Kolmogorov-Smirnov test.

3. Results

We first analyze the ENSO response in the first winter, i.e. 6-9 months after the start of the eruption, and then turn to the changes in the second and third year after the eruption.

3.1. ENSO response in the winter following the eruption

Our results show that the simulated high-latitude volcanic eruption gives rise to anomalous El Niño-like conditions in the tropical Pacific, peaking 4 to 9 months after the eruption starts (Fig. 1b, c). For an eruption that is imposed during incipient La Niña conditions in the no-volcano simulation, the probability of a La Niña event in the following winter shifts from 100% in the no-volcano case (by construction) to 45% in the volcano case, while the probability of having an El Niño becomes 15% (Tables 1 and S1). The probability of an extreme La Niña (Niño3.4 index $< -1.2^{\circ}\text{C}$) is suppressed, passing from 30% in the no-volcano case to 5% after the imposed eruption. In the incipient La Niña case, the probability of a strong El Niño ($0.8 < \text{Niño3.4 index} < 1.2^{\circ}\text{C}$) in the first winter following the eruption becomes non-zero although very small (Tables 1 and S1). For a volcanic event that is imposed during incipient neutral conditions in the no-volcano simulation, the probability of

an El Niño event jumps to 72%, with a 25% chance of an extreme El Niño event. Finally, for El Niño incipient conditions the probability of having extreme El Niño and strong El Niño events shifts respectively from 30% and 20% in the no-volcano case to 35% and 25% in the volcano case (Tables 1 and S1).

The El Niño-like anomaly is triggered by the NH cooling associated to the volcanic eruption. The NH cooling moves the zonal average ITCZ southward over the Pacific (Fig 1a), causing the zonal component of the trade winds to relax. This in turn gives rise to El Niño-like anomalies (Fig. 1b, c), as shown by *Pausata et al.* [2015b]. Interestingly, while the ITCZ shift is similar in all three cases ($\sim 5\text{-}6^\circ$ latitude, Fig. 1a), the changes in precipitation as well as wind anomalies over the Tropical Pacific are remarkably weaker in the incipient El Niño relative to the incipient La Niña ensemble (Fig. 2). The incipient Neutral and La Niña ensembles instead show similar anomaly patterns for the winter following the eruption (cf. panel c and d in Fig. 1). As a consequence the El Niño-like anomalies are significantly stronger in the incipient La Niña and Neutral cases compared to the incipient El Niño case (Figs 1b, c, and 3).

This asymmetry of the response is plausible since there is an upper limit to the absolute intensity of an El Niño event, so there is more room for large anomalies when starting from Neutral or La Niña conditions. However, there are more subtle effects at play as well. Firstly, the incipient La Niña and Neutral cases have a stronger Bjerknes feedback compared to the incipient El Niño cases [*Bjerknes*, 1969]. In incipient La Niña (and Neutral) conditions the ITCZ is farther north (dashed lines in Fig. 1a) and the trades on the equator are stronger relative to the incipient El Niño case (Fig. 2). Given the quadratic relationship between wind speed and wind stress, a nominal zonal wind anomaly along the equator will therefore lead to a larger change in wind stress under incipient La Niña than incipient El Niño conditions. Moreover, the westerly wind speed anomaly is itself stronger when the volcanic forcing acts

during incipient La Niña events (Fig. S3b, f). Both these factors lead to the much stronger equatorial wind stress anomalies seen in the La Niña than in the El Niño case (Fig. 2b, f).

Another factor that makes the incipient La Niña conditions more sensitive to the volcanic eruption is the tropical Pacific ocean state. During incipient La Niña and neutral conditions, in the Eastern Pacific the upper ocean temperature stratification is stronger, the thermocline is shallower and zonal SST gradients are larger than in the El Niño case (Figs. S1 and S2). Hence, in the La Niña case wind stress perturbations more readily generate changes in SST via anomalous advection and upwelling, which are also less effectively damped (a more detailed discussion can be found in the supporting information: see figure S4 and *Battisti*, [1988], *Battisti and Hirst* [1989], and *Im et al.* [2015]). Therefore, the volcanically-induced wind stress anomalies more efficiently perturb the system under incipient La Niña and neutral conditions than under incipient El Niño events.

3.2. ENSO response in the second and third year after the eruption

The impact of a high-latitude volcanic eruption on the evolution of the ENSO is evident for about three years after the eruption (Fig. 3), depending on the ENSO state at the time of the eruption. When the volcano erupts during the incipient stage of an El Niño event, the year after the eruption (YEAR02) is characterized by strong La Niña-like anomalies and no SST anomalies are simulated beyond the second year after the eruption (YEAR03). When the volcano erupts during an incipient La Niña, the strong El Niño-like anomalies that develop in the year of the eruption are followed by near-neutral conditions in year two, and La Niña-like anomalies in year three (Fig. 3). The Neutral case lies somewhere in between El Niño and La Niña cases (Fig. 3b).

The La Niña-like anomalies that appear in the second year following an eruption during the incipient stage of an El Niño event (and during neutral conditions) are not a consequence of the general post-eruption cooling but are dynamically driven, as can be seen by the sub-

surface ocean temperature anomalies (cf. Figs. S2 and S5). The sub-surface ocean anomalies clearly show a La Niña-like pattern in the second year after the eruption occurring during the incipient phase of an El Niño event and during Neutral cases, and in the third year after an eruption during incipient La Niña conditions. In general, our results show increased likelihood of La Niña events in the second and third year after the volcanic eruption (Tables 1 and S1).

In the absence of volcanic forcing (no-volcano ensemble), strong El Niño events in our model are generally followed by La Niña winters in the following year (Fig. 4a, b), whereas weaker El Niños slowly fade and La Niña conditions develop only after 3 years (Fig. 4a). An analysis of the Extended Reconstructed Sea Surface Temperature (ERSST) data set (see supporting information and *Smith et al.* [2008]) show that ENSO behaviors in our model are in qualitative agreement with that in observation (see supporting information): strong El Niño events rapidly transition towards negative ENSO anomalies within a year; La Niña events shift toward an El Niño only three years after, whereas in the model this occurs after two years (Fig. S6).

Thus, when a volcanic eruption occurs under an incipient El Niño, the additional El Niño-like anomaly gives rise to stronger El Niño events that are more prone to developing La Niña-like conditions on the following year (cf. Figs. 2b and 4b). When the volcanic eruption instead takes place under an incipient La Niña, the Niño-like anomaly largely cancels the negative anomaly, bringing the ENSO state towards neutral conditions (Fig. 3). This change in ENSO state naturally leads to a different ENSO behavior compared to the original no-volcano case (Fig. 4c): La Niña events are in general followed by El Niño events after about two years, whereas neutral/slightly cold (negative) states develop into negative anomalies. Therefore, the La Niña-like conditions on the third year after the eruption are just a response to the change in initial ENSO mean state due to the eruption (from La Niña to neutral

conditions, cf. Figs. 3b and 4d).

4. Discussion and Conclusions

Our study used a large ensemble ($n=60$) to demonstrate that a summertime high-latitude eruption in the Northern Hemisphere impacts the subsequent evolution of the tropical Pacific atmosphere and ocean system (i.e. the state of ENSO) for up to three years following the eruption. The response is strongly sensitive to the phase of the ENSO mode at the time of the eruption. In particular, our simulations show that summer high-latitude volcanic eruptions in the Northern Hemisphere trigger an El Niño-like anomaly in the following winter; this response is stronger if the eruption occurs in a summer with developing La Niña or Neutral conditions compared to a summer with developing El Niño conditions. During incipient La Niña conditions, the ITCZ is further north and the equatorial surface easterlies are stronger relative to incipient El Niño conditions (Fig. 1). As a result, the same ITCZ latitudinal displacement leads to a stronger westerly surface wind stress anomaly in the La Niña case than in El Niño case (Fig. 2). In addition, during incipient La Niña conditions, the tropical Pacific zonal SST gradient and the upwelling are stronger relative to the El Niño case (Figs. S1 and S2), making the atmosphere-ocean coupling stronger [Bjerknes, 1969], while atmospheric damping is less efficient (Fig. S4).

While many studies have investigated the ENSO response to volcanic eruptions, most of them have focused on tropical eruptions [Mann *et al.*, 2005; Emile-Geay *et al.*, 2008; McGregor and Timmermann, 2011; Ohba *et al.*, 2013; Ding *et al.*, 2014; Maher *et al.*, 2015], with the exception of Pausata *et al.* [2015b] and Stevenson *et al.* [2016], who also considered high-latitude eruptions. Furthermore, only one study has previously examined the sensitivity of the ENSO response to volcanic eruptions as a function of the ENSO phase at the time of the eruption [Ohba *et al.*, 2013]. In agreement with our study, Ohba *et al.* [2013] found a stronger ENSO response in the winter after the eruption during La Niña than El Niño events,

but they examined tropical eruptions only. Using a coupled climate model, they found no response when the eruption occurs in an El Niño case, but conversely simulate a large El Niño-like anomaly during La Niña case (anomaly up to $\sim 0.7^{\circ}\text{C}$; see Fig. 6b in *Ohba et al.* [2013]). This suggests that the ENSO response is highly sensitive to the initial state of the tropical Pacific atmosphere-ocean system at the time of the eruption.

Our results show that the impact of NH high-latitude volcanic eruptions on ENSO also extends to the second and third year after the eruption (Fig. 3), showing opposite behavior in the El Niño and La Niña case. When the eruption occurs during the development stage of an El Niño, the year after the eruption (YEAR02) is characterized by La Niña-like anomalies compared to the no-volcano ensemble. When a summer eruption takes place during an incipient La Niña, the El Niño-like anomalies that develop in the year of the eruption (YEAR01) are followed by near neutral conditions (YEAR02), and then by La Niña-like anomalies (YEAR03). Overall, the probability of La Niña events increases in the second and third year after the eruption (Tables 1 and S1). Interestingly, recent modelling studies [*Zanchettin et al.*, 2012; *Maher et al.*, 2015] also show a La Niña-like anomaly occurring three years after the eruption. These findings are consistent with the results from the proxy-based study of *McGregor et al.* [2010], who find evidence of a La Niña pattern developing approximately three years post eruption. In a modelling study, *Pausata et al.* [2015b] also report a La Niña-like anomaly in the third year after the eruption when the ENSO phases are clustered together (see Fig. 1C and S5 in *Pausata et al.* [2015b]).

In a recent study, *Stevenson et al.* [2016] examine the response to eruptions in the last millennial simulation using the CESM1.1. They report a similar result for the first year as we find using the NorESM1-M (see Fig. 1 and [*Pausata et al.*, 2015b]): a NH eruption in boreal spring/summer causes El Niño-like anomalies six to nine months later. In contrast to our results that show neutral or La Niña-like anomalies on the second year, their El Niño-like

anomalies extend throughout the following year (YEAR02). These differences likely stem from differences in the ENSO dynamics in the two models: in CESM1.1 ENSO has too much variance and a period that is too long compared to observations [Stevenson *et al.*, 2016]; NorESM1-M does not feature such biases [Bellenger *et al.*, 2014]. These biases may be the cause of the differences in the two models' second-year response to volcanic forcing.

The above-mentioned studies do not differentiate the response as a function of the incipient state of ENSO at the time of the eruption; rather, they report the composite response to all eruptions. The results reported in the present work stress the importance of separating the initial ENSO states when investigating its response to volcanic eruption. The ENSO response to high-latitude volcanic eruptions is also likely to depend on the season in which the eruption occurs. We anticipate that aerosol loading that is hemispherically asymmetric would have its greatest impact on ENSO when the loading occurs during NH spring and early summer because the ENSO mode is most sensitive to perturbations applied in April through August [Thompson and Battisti, 2000]. Moreover, it takes approximately two-to-three months for the eruption to displace the ITCZ southward in the Pacific due to the thermal inertia of the upper ocean (see Fig. S3 in Pausata *et al.* [2015b]). Aerosol loading in the NH in winter (October to January) will have a comparatively weak impact on ENSO because the insolation is low (less forcing) and the ENSO mode is least sensitive to perturbations in NH winter. Further studies investigating the seasonal dependence of the ENSO response to high-latitude volcanic eruption will be necessary to validate this hypothesis.

New proxy archives, helping to constrain past ENSO variability, are increasingly becoming available, and our results provide a modeling framework for a better interpretation of these data. Our results also serve as a framework for understanding the response of ENSO in climate models that simulate the Last Millennium and to those proposed in the Volcano Model Intercomparison Project [Zanchettin *et al.*, 2016]. Given that ENSO is the major

component of tropical climate variability and is known to affect global climate and weather extremes [Ropelewski and Halpert, 1987], these and other similar studies will prove valuable to society for improving mitigation of climate anomalies that result from high-latitude volcanic eruptions in the Northern Hemisphere.

Acknowledgments

We would like to thank Sylvia Dee and another anonymous reviewer for helpful comments on the manuscript. FSRP is funded by Sweden's Vetenskapsrådet, as part of the MILEX project. The simulations were performed on resources provided by the Swedish National Infrastructure for Computing (SNIC) at NSC. C.K. is supported by U.S. NSF grants OCN-1304910 and AGS-1602097. Data used in this paper may be obtained upon request to F.S.R.P. (francesco.pausata@misu.su.se).

Author contributions

F.S.R.P. conceived and designed the study, carried out the experiments, analyzed the model outputs and led the writing. C.K. analyzed the model output. C.K., R.C. and D.S.B. contributed to the interpretation of the model results. All authors contributed to the writing of the manuscript.

References

- Adams, J. B., M. E. Mann, and C. M. Ammann (2003), Proxy evidence for an El Niño-like response to volcanic forcing., *Nature*, *426*(6964), 274–8, doi:10.1038/nature02101.
- Battisti, D. S. (1988), Dynamics and Thermodynamics of a Warming Event in a Coupled Tropical Atmosphere–Ocean Model, *J. Atmos. Sci.*, *45*(20), 2889–2919, doi:10.1175/1520-0469(1988)045<2889:DATOAW>2.0.CO;2.
- Battisti, D. S., and A. C. Hirst (1989), Interannual Variability in a Tropical Atmosphere–Ocean Model: Influence of the Basic State, Ocean Geometry and Nonlinearity, *J. Atmos. Sci.*, *46*(12), 1687–1712, doi:10.1175/1520-0469(1989)046<1687:IVIATA>2.0.CO;2.
- Bellenger, H., E. Guilyardi, J. Leloup, M. Lengaigne, and J. Vialard (2014), ENSO representation in climate models: from CMIP3 to CMIP5, *Clim. Dyn.*, *42*(7-8), 1999–2018, doi:10.1007/s00382-013-1783-z.
- Bentsen, M. et al. (2013), The Norwegian Earth System Model, NorESM1-M – Part 1: Description and basic evaluation of the physical climate, *Geosci. Model Dev.*, *6*(3), 687–720, doi:10.5194/gmd-6-687-2013.
- Bjerknes, J. (1969), Atmospheric teleconnections from the equatorial Pacific, *Mon. Weather Rev.*, *97*(3), 163–172, doi:10.1175/1520-0493(1969)097<0163:ATFTEP>2.3.CO;2.
- Caballero, R., and B. T. Anderson (2009), Impact of midlatitude stationary waves on regional Hadley cells and ENSO, *Geophys. Res. Lett.*, *36*(17), L17704, doi:10.1029/2009GL039668.
- Clement, A. C., R. Seager, M. A. Cane, and S. E. Zebiak (1996), An Ocean Dynamical Thermostat, *J. Clim.*, *9*(9), 2190–2196, doi:10.1175/1520-0442(1996)009<2190:AODT>2.0.CO;2.
- D'Arrigo, R., R. Wilson, and A. Tudhope (2008), The impact of volcanic forcing on tropical temperatures during the past four centuries, *Nat. Geosci.*, *2*(1), 51–56, doi:10.1038/ngeo393.

- D'Arrigo, R., R. Seager, J. E. Smerdon, A. N. LeGrande, and E. R. Cook (2011), The anomalous winter of 1783–1784: Was the Laki eruption or an analog of the 2009–2010 winter to blame?, *Geophys. Res. Lett.*, *38*(5), L05706, doi:10.1029/2011GL046696.
- Ding, Y., J. A. Carton, G. A. Chepurin, G. Stenchikov, A. Robock, L. T. Sentman, and J. P. Krasting (2014), Ocean response to volcanic eruptions in Coupled Model Intercomparison Project 5 (CMIP5) simulations, *J. Geophys. Res. Ocean.*, *119*(9), 5622–5637, doi:10.1002/2013JC009780.
- Emile-Geay, J., R. Seager, M. A. Cane, E. R. Cook, and G. H. Haug (2008), Volcanoes and ENSO over the Past Millennium, *J. Clim.*, *21*(13), 3134–3148, doi:10.1175/2007JCLI1884.1.
- Finnsón, H. (1796), *Mannfækkun af hallærum (Decimation of the population in Iceland)*, in *Rit þess konunglega íslenska Lærdómslistafélags*, Almenna Bókafélagið, Reykjavík.
- Gregory, J. M. (2010), Long-term effect of volcanic forcing on ocean heat content, *Geophys. Res. Lett.*, *37*(22), L22701, doi:10.1029/2010GL045507.
- Highwood, E. J., and D. S. Stevenson (2003), Atmospheric impact of the 1783 – 1784 Laki Eruption: Part II Climatic effect of sulphate aerosol, *Atmos. Chem. Phys.*, *3*, 1177–1189.
- Hirono, M. (1988), On the trigger of El Niño Southern Oscillation by the forcing of early El Chichón volcanic aerosols, *J. Geophys. Res.*, *93*(D5), 5365, doi:10.1029/JD093iD05p05365.
- Im, S.-H., S.-I. An, S. T. Kim, and F.-F. Jin (2015), Feedback processes responsible for El Niño-La Niña amplitude asymmetry, *Geophys. Res. Lett.*, *42*(13), 5556–5563, doi:10.1002/2015GL064853.
- Iversen, T. et al. (2013), The Norwegian Earth System Model, NorESM1-M – Part 2: Climate response and scenario projections, *Geosci. Model Dev.*, *6*(2), 389–415, doi:10.5194/gmd-6-389-2013.
- Kravitz, B., and A. Robock (2011), Climate effects of high-latitude volcanic eruptions: Role of the time of year, *J. Geophys. Res.*, *116*(D1), D01105, doi:10.1029/2010JD014448.
- Landrum, L., B. L. Otto-Bliesner, E. R. Wahl, A. Conley, P. J. Lawrence, N. Rosenbloom, and H. Teng (2013), Last Millennium Climate and Its Variability in CCSM4, *J. Clim.*, *26*(4), 1085–1111, doi:10.1175/JCLI-D-11-00326.1.
- Maher, N., S. McGregor, M. H. England, and A. Sen Gupta (2015), Effects of volcanism on tropical variability, *Geophys. Res. Lett.*, *42*(14), n/a–n/a, doi:10.1002/2015GL064751.
- Mann, M. E., M. A. Cane, S. E. Zebiak, and A. Clement (2005), Volcanic and Solar Forcing of the Tropical Pacific over the Past 1000 Years, *J. Clim.*, *18*(3), 447–456, doi:10.1175/JCLI-3276.1.
- McGregor, S., and A. Timmermann (2011), The Effect of Explosive Tropical Volcanism on ENSO, *J. Clim.*, *24*(8), 2178–2191, doi:10.1175/2010JCLI3990.1.
- McGregor, S., A. Timmermann, and O. Timm (2010), A unified proxy for ENSO and PDO variability since 1650, *Clim. Past*, *6*(1), 1–17, doi:10.5194/cp-6-1-2010.
- Neale, R. B., J. Richter, S. Park, P. H. Lauritzen, S. J. Vavrus, P. J. Rasch, and M. Zhang (2013), The Mean Climate of the Community Atmosphere Model (CAM4) in Forced SST and Fully Coupled Experiments, *J. Clim.*, *26*(14), 5150–5168, doi:10.1175/JCLI-D-12-00236.1.
- Ohba, M., H. Shiogama, T. Yokohata, and M. Watanabe (2013), Impact of Strong Tropical Volcanic Eruptions on ENSO Simulated in a Coupled GCM, *J. Clim.*, *26*, 5169–5182.
- Oman, L., A. Robock, G. L. Stenchikov, G. A. Schmidt, and R. Ruedy (2005), Climatic response to high-latitude volcanic eruptions, *J. Geophys. Res.*, *110*(D13), D13103, doi:10.1029/2004JD005487.
- Oman, L., A. Robock, G. L. Stenchikov, and T. Thordarson (2006a), High-latitude eruptions cast shadow over the African monsoon and the flow of the Nile, *Geophys. Res. Lett.*, *33*(18), L18711, doi:10.1029/2006GL027665.
- Oman, L., A. Robock, G. L. Stenchikov, T. Thordarson, D. Koch, D. T. Shindell, and C. Gao (2006b), Modeling the distribution of the volcanic aerosol cloud from the 1783–1784 Laki eruption, *J. Geophys. Res.*, *111*(D12), D12209, doi:10.1029/2005JD006899.
- Pausata, F. S. R., A. Grini, R. Caballero, A. Hannachi, and Ø. Seland (2015a), High-latitude volcanic

- eruptions in the Norwegian Earth System Model: the effect of different initial conditions and of the ensemble size, *Tellus B*, 67(26728).
- Pausata, F. S. R., L. Chafik, R. Caballero, and D. S. Battisti (2015b), Impacts of high-latitude volcanic eruptions on ENSO and AMOC, *Proc. Natl. Acad. Sci.*, 201509153, doi:10.1073/pnas.1509153112.
- Robock, A. (2000), Volcanic eruptions and climate, *Rev. Geophys.*, 38(2), 191–219.
- Ropelewski, C. F., and M. S. Halpert (1987), Global and Regional Scale Precipitation Patterns Associated with the El Niño/Southern Oscillation, *Mon. Weather Rev.*, 115(8), 1606–1626, doi:10.1175/1520-0493(1987)115<1606:GARSPP>2.0.CO;2.
- Schmidt, A., T. Thordarson, L. D. Oman, A. Robock, and S. Self (2012), Climatic impact of the long-lasting 1783 Laki eruption: Inapplicability of mass-independent sulfur isotopic composition measurements, *J. Geophys. Res.*, 117(D23), D23116, doi:10.1029/2012JD018414.
- Smith, T. M., R. W. Reynolds, T. C. Peterson, and J. Lawrimore (2008), Improvements to NOAA's Historical Merged Land–Ocean Surface Temperature Analysis (1880–2006), *J. Clim.*, 21(10), 2283–2296, doi:10.1175/2007JCLI2100.1.
- Stevenson, S., B. Otto-Bliesner, J. Fasullo, and E. Brady (2016), “El Niño Like” Hydroclimate Responses to Last Millennium Volcanic Eruptions, *J. Clim.*, 29(8), 2907–2921, doi:10.1175/JCLI-D-15-0239.1.
- Thompson, C. J., and D. S. Battisti (2000), A Linear Stochastic Dynamical Model of ENSO. Part I: Model Development, *J. Clim.*, 13(15), 2818–2832, doi:10.1175/1520-0442(2000)013<2818:ALSDMO>2.0.CO;2.
- Vimont, D. J., D. S. Battisti, and A. C. Hirst (2001), Footprinting: A seasonal connection between the tropics and mid-latitudes, *Geophys. Res. Lett.*, 28(20), 3923–3926, doi:10.1029/2001GL013435.
- Wood, C. A. (1992), *Climatic effects of the 1783 Laki eruption, in The Year Without a Summer: World Climate in 1816*, edited by C.R. Harrington, Can. Mus. of Nat. , Ottawa.
- Zanchettin, D., C. Timmreck, H.-F. Graf, A. Rubino, S. Lorenz, K. Lohmann, K. Krüger, and J. H. Jungclauss (2012), Bi-decadal variability excited in the coupled ocean–atmosphere system by strong tropical volcanic eruptions, *Clim. Dyn.*, 39(1-2), 419–444, doi:10.1007/s00382-011-1167-1.
- Zanchettin, D. et al. (2016), The Model Intercomparison Project on the climatic response to Volcanic forcing (VolMIP): Experimental design and forcing input data, *Geosci. Model Dev. Discuss.*, 1–33, doi:10.5194/gmd-2016-68.

Table 1: Changes in probability of the occurrence of an El Niño, a Neutral or a La Niña event conditional on incipient ENSO state in the three winters following the eruption for the volcano relative to no-volcano ensemble. Also shown in the bottom four rows is the probability change for strong (Niño3.4 index between 0.8°C and 1.2°C in absolute values, i.e. Niño3.4 index standard deviation between 1 and 2) and extreme (Niño3.4 index greater than 1.2°C in absolute values, i.e. Niño3.4 index standard deviation greater than 2) events. The term “incipient ENSO state” refers to the ENSO state in DJF of YEAR01 in the historical no-volcano simulation. By construction, in the no-volcano ensemble the probability of El Niño, Neutral and La Niña events equals 100% for the first winter following the eruption (YR01) in the incipient El Niño, Neutral and La Niña state, respectively. The Neutral, El Niño and La Niña cases are composed respectively of 20, 18 and 22 members. Statistically significant changes at 95% confidence level are shown in bold (red positive, blue negative); significance is calculated with a bootstrap technique using an extended historical control simulation (1850-1999; see supporting information). The symbol “–” indicates no change.

Incipient ENSO state \ Probability of event	El Niño			Neutral			La Niña		
	YR01	YR02	YR03	YR01	YR02	YR03	YR01	YR02	YR03
El Niño	-5%	-6%	-6%	+72%	-25%	-20%	+15%	–	-13%
Neutral	+5%	-11%	-11%	-72%	+15%	+10%	+40%	-13%	+3%
La Niña	–	+17%	+17%	–	+10%	+5%	-55%	+13%	+10%
strong El Niño 0.8°C < Niño3.4 < 1.2°C	+5%	+5%	-11%	+25%	–	-5%	+5%	-5%	–
extreme El Niño Niño3.4 > 1.2°C	+5%	-5%	-5%	–	-15%	-15%	–	+5%	-10%
strong La Niña -1.2°C < Niño3.4 < -0.8°C	–	-11%	–	–	-10%	+15%	+5%	+18%	–
extreme La Niña Niño3.4 < -1.2°C	–	+34%	+11%	–	+15%	-5%	-25%	–	+14%

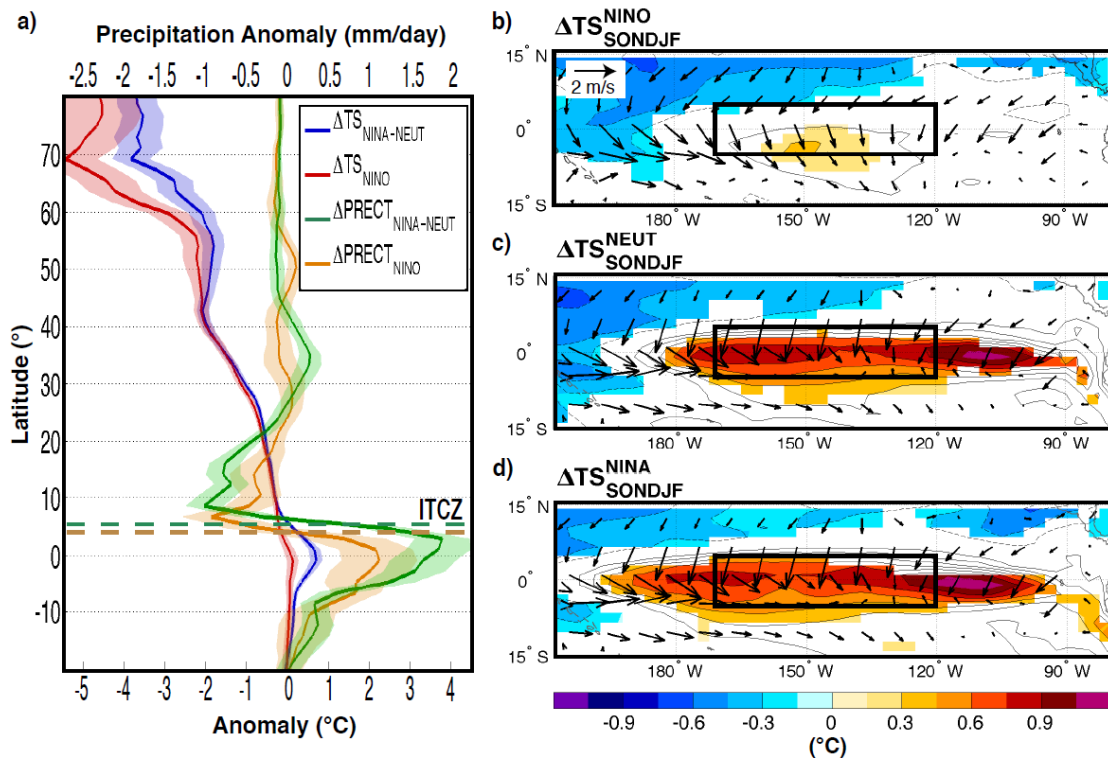


Figure 1: a) Changes in the zonal-mean surface temperature (red and blue) and precipitation (brown and green) between the volcano (ENS_v) and no-volcano (ENS_{nv}) ensemble over the Pacific Ocean (150°E–90°W) for the El Niño and La Niña-Neutral cases in the 4 to 9 months after the beginning of the eruption (September to February). Shading represents twice the standard error of the mean (approximate 95% confidence intervals). The bold brown and green dashed lines highlight the ensemble-averaged position of the ITCZ (defined as the location of the zonal-average precipitation maximum) in the no-volcano simulations for the El Niño and La Niña-Neutral cases, respectively. b) Changes in near surface wind (arrows) and sea surface temperature (shading) for the El Niño, c) Neutral and d) La Niña cases between the ENS_v and ENS_{nv} ensemble in the 4 to 9 months after the beginning of the eruption. The box indicates the Niño3.4 area. Contours show the SST anomalies following the colorbar scale (solid lines for positive anomalies and dashed lines for negative anomalies). Only significant SST changes are significant at 95% confidence level using a k -s test.

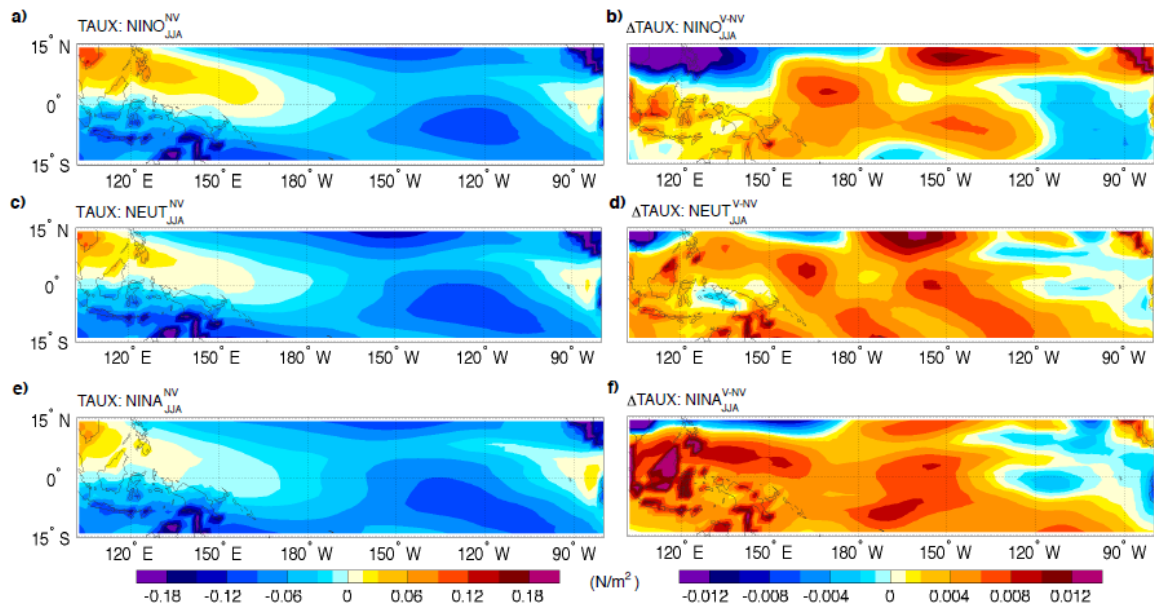


Figure 2: Climatological zonal wind stress in the no-volcano ensemble (a, c, e) and the volcanically induced changes (b, d, f) for the Niño, Neutral and Niña cases in the summer (June to August, JJA) over the Tropical Pacific.

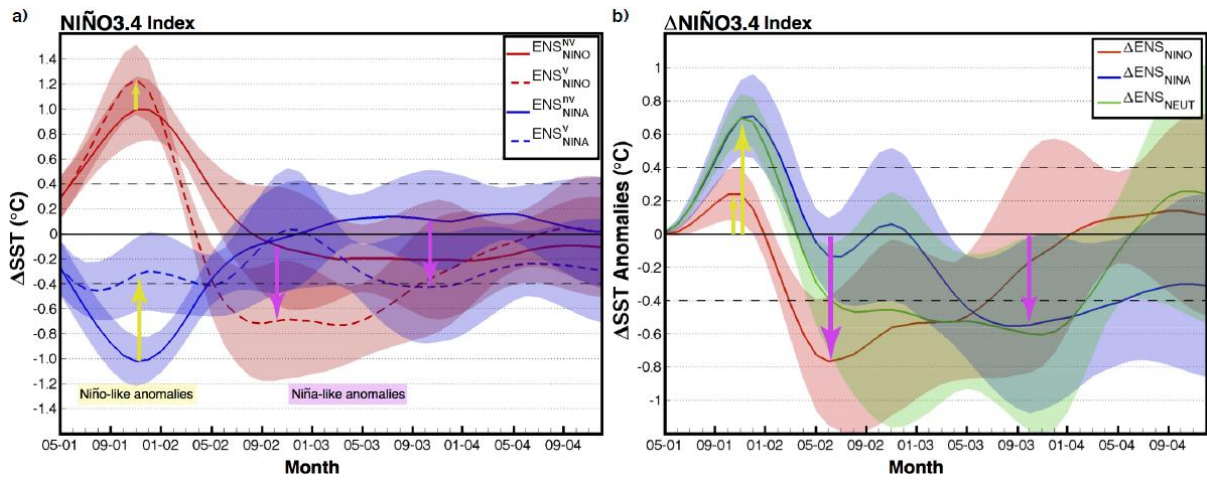


Figure 3: a) Niño3.4 index for incipient El Niño and incipient La Niña ensemble for the volcano and no-volcano cases. The Niño-like and Niña-like text legends highlight the ENSO anomalies occurring in the first year and in the following year respectively; b) The change in the Niño3.4 index (volcano minus no-volcano experiments) for the incipient El Niño, La Niña and Neutral cases. For clarity, the neutral case has been omitted in panel a). Shading represents twice the standard error of the mean (approximate 95% confidence intervals).

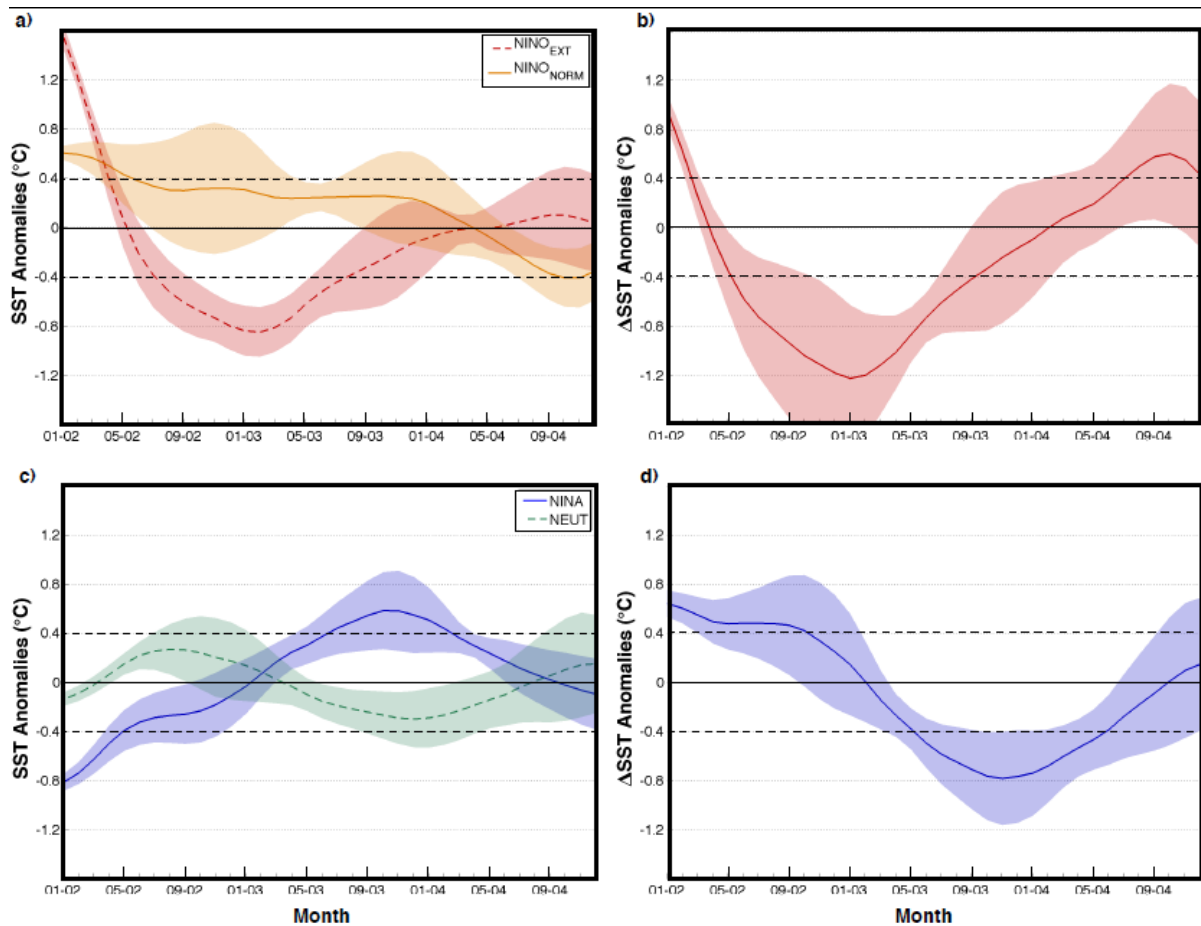


Figure 4: Composite of Niño3.4 index for very strong (Niño3.4 index $> 1.2^{\circ}\text{C}$, NINO_{EXT}) and moderate ($0.4 < \text{Niño3.4 index} < 0.8^{\circ}\text{C}$, $\text{NINO}_{\text{NORM}}$) El Niño events in the no-volcano ensemble (a), and their difference (b). Composite of Niño3.4 index for neutral/slightly negative ($-0.4^{\circ}\text{C} < \text{Niño3.4 index} < 0.2^{\circ}\text{C}$) and moderate/strong ($-1.2 < \text{Niño3.4 index} < -0.6^{\circ}\text{C}$) La Niña events in the no-volcano ensemble (c), and their difference (d). The choice of the intervals is made to facilitate the comparison to the changes in the initial ENSO state induced by the volcanic eruption. Shading represents twice the standard error of the mean (approximate 95% confidence intervals).